

**Enhanced photon blockade via driving a trapped  $\Lambda$ -type atom in a hybrid optomechanical system**Dong-Yang Wang,<sup>1</sup> Cheng-Hua Bai,<sup>1</sup> Yan Xing,<sup>1</sup> Shutian Liu <sup>1,\*</sup> Shou Zhang,<sup>2,†</sup> and Hong-Fu Wang <sup>2,‡</sup><sup>1</sup>*School of Physics, Harbin Institute of Technology, Harbin, Heilongjiang 150001, China*<sup>2</sup>*Department of Physics, College of Science, Yanbian University, Yanji, Jilin 133002, China*

(Received 1 June 2020; revised 14 September 2020; accepted 21 September 2020; published 13 October 2020)

A scheme is proposed to enhance the photon blockade effect in a hybrid optomechanical system with a  $\Lambda$ -type atom driven by the microwave. Through analyzing the conventional and unconventional blockade mechanisms, we find that the enhanced photon blockade effect can be attributed to two aspects: (i) The nonresonant coupled  $\Lambda$ -type atom reconstructs the anharmonic eigenenergy spectrum and (ii) the microwave driving field promotes the destructive quantum interference for two-photon excitation. By means of the joint enhancement effect, the perfect photon blockade, i.e., the second-order correlation function  $g^{(2)}(0) \simeq 0$ , can be achieved without the strong single-photon optomechanical coupling as reported in the standard optomechanical system. All the analyses and derivations are further verified via simulating numerically the quantum master equation of the initial Hamiltonian, showing good agreement between analytical and numerical results. Moreover, the optimal parameter relation is given to optimize the photon blockade and maximize the occupancy probability of single-photon excitation at the same time. Our scheme provides a feasible method to engineer a high-quality and efficient single-photon source.

DOI: [10.1103/PhysRevA.102.043705](https://doi.org/10.1103/PhysRevA.102.043705)**I. INTRODUCTION**

Over the past decades, optomechanics [1–6], investigating light-matter interaction, has attracted extensive attention to explore various questions of quantum mechanics on the macroscopic scale, such as mechanical cooling [7–12], squeezing [13–16], entanglement [17,18], and quantum superposition state [19–21]. In contrast, mechanical motion also affects the optical mode, which triggers some interesting phenomena, e.g., optical amplification [22,23], optomechanically induced transparency [24–27], nonreciprocity [28], the Casimir effect [29], and photon blockade [30–34]. Note that nonreciprocal photon blockade has already been predicted [35,36] and confirmed experimentally [37]. Among these studies, the photon blockade, the occupation of the first photon blocking the consequent injection, is a nonclassical antibunching effect, which can be used to generate the single-photon source for those fundamental studies in quantum information processing and quantum optics fields [38,39]. Therefore, how to achieve a strong photon blockade has been a hot subject in the recent years.

A conventional photon blockade mechanism of relying on the eigenenergy spectrum has been proposed [40–42] and realized in experiments [43,44]. However, the conventional photon blockade in an optomechanical system (OMS) has not been reported experimentally due to the required excessive single-photon optomechanical coupling [30,31]. On the other hand, an unconventional photon blockade mecha-

nism, based on the destructive quantum interference between different excitation paths [45–51], has been observed experimentally in a coupled quantum-dot-cavity system [52] and a superconducting circuit system [53]. According to the new unconventional photon blockade mechanism, the auxiliary cavity mode [36,54–57] or parametric amplification [58] method was proposed to break the usual limit, in which the strong photon blockade can be effectively achieved even with a weak optomechanical coupling. This can be explained by the fact that the presence of the auxiliary qubit constructs another transition path to achieve the destructive quantum interference of two-photon excitation. Analogous to the photon blockade, the phonon blockade has also been studied in various nanomechanical systems [59–62].

Furthermore, there are some related studies about the photon blockade in the hybrid OMS, such as coupling a two-level system to the mechanical mode [63] and trapping a third-order nonlinear medium in the optomechanical cavity [64]. This paper comprises the strategy to enhance the photon blockade effect with a trapped  $\Lambda$ -type atom in a hybrid OMS [65–67]. By calculating the second-order correlation function of photons analytically and numerically, we find a two-step enhancement phenomenon of photon blockade. First, the nonresonant coupled atom not only shifts the anharmonic energy level, but also changes the size of energy splitting between the higher and lower branches of eigenstates, which results in a finite enhancement of the photon blockade effect. Second, the microwave field acting on the atom further promotes the photon antibunching effect by improving the destructive quantum interference. Under the interplay of nonresonant coupled atoms and a microwave driving field, the strong photon blockade can be obtained even when the single-photon optomechanical coupling is much smaller than the mecha-

\*stliu@hit.edu.cn

†szhang@ybu.edu.cn

‡hfwang@ybu.edu.cn

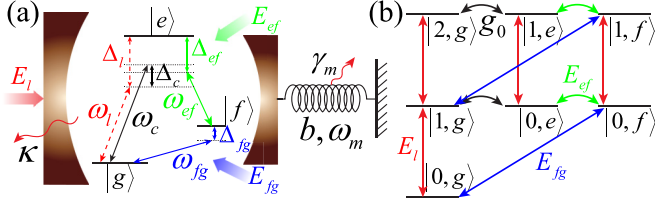


FIG. 1. (a) Schematic diagram of the hybrid OMS with a trapped  $\Lambda$ -type atom, which includes two hyperfine ground states  $\{|g\rangle, |f\rangle\}$  and an excited state  $|e\rangle$ . (b) Transition  $|g\rangle \leftrightarrow |e\rangle$  coupled to the  $\sigma$ -polarized optical cavity with coupling coefficient  $g_0$ . A  $\pi$ -polarized classical laser field is applied to drive the transition  $|f\rangle \leftrightarrow |e\rangle$  with Rabi frequency  $E_{ef}$ . The transition  $|g\rangle \leftrightarrow |f\rangle$  is driven by a microwave field with Rabi frequency  $E_{fg}$ . In addition, the cavity mode is pumped by a laser field with amplitude  $E_l$ . The frequency and detuning of different driving fields are illustrated.

ical frequency. We analytically derive the optimal parameter relation, which agrees well with the numerical simulation of the initial Hamiltonian. Meanwhile, the necessity of microwave driving field is also demonstrated by calculating the correlation function analytically in the absence of the microwave field. Moreover, to ensure the quality and efficiency of single-photon emission, we discuss how to maximize the intracavity photon number when the strong photon blockade occurs. Therefore, our scheme greatly reduces the required optomechanical coupling to achieve a strong photon blockade and provides an alternative way for the experimental implementation of photon blockade.

The rest of paper is organized as follows. In Sec. II we illustrate the hybrid OMS with a trapped  $\Lambda$ -type atom and derive the Hamiltonian of the system under the large detuning condition. In Sec. III we calculate the second-order correlation function analytically and numerically and give the optimal parameter relation to optimize the photon blockade effect. In addition, we discuss the enhanced photon blockade. A summary is given in Sec. IV.

## II. SYSTEM AND HAMILTONIAN

As depicted in Fig. 1(a), we consider a hybrid OMS, where a  $\Lambda$ -type three-level atom is trapped in the optical cavity consisting of a fixed mirror and a movable one. The required atomic level configuration can use the  $^{87}\text{Rb}$  atom [68–71], where states  $|g\rangle$ ,  $|f\rangle$ , and  $|e\rangle$  are represented by the hyperfine atomic levels  $|5^2S_{1/2}, F=1, m=0\rangle$ ,  $|5^2S_{1/2}, F=1, m=-1\rangle$ , and  $|5^2P_{1/2}, F=1, m=-1\rangle$ , respectively. The Hamiltonian of the system is written as ( $\hbar=1$ )

$$H_s = \omega_c a^\dagger a + \omega_m b^\dagger b + \omega_f |f\rangle\langle f| + \omega_e |e\rangle\langle e| + g_0(a^\dagger |g\rangle\langle e| + a|e\rangle\langle g|) - ga^\dagger a(b^\dagger + b), \quad (1)$$

where the first four terms represent the free Hamiltonian of the optical cavity, the mechanical oscillator, and the atom. Here we have chosen the energy of level  $|g\rangle$  as the zero potential energy point. The fifth term describes the interaction between the atom and optical cavity with coupling strength  $g_0$ . The last term is the optomechanical interaction with single-photon coupling strength  $g$ . Meanwhile, the considered system is

driven by three classical laser fields and the Hamiltonian is

$$H_d = E_l e^{i\phi_l} a^\dagger e^{-i\omega_l t} + E_{ef} e^{i\phi_{ef}} |e\rangle\langle f| e^{-i\omega_{ef} t} + E_{fg} e^{i\phi_{fg}} |f\rangle\langle g| e^{-i\omega_{fg} t} + \text{H.c.}, \quad (2)$$

where the first term represents the pumping-cavity interaction with pumping amplitude  $E_l$ , frequency  $\omega_l$ , and phase  $\phi_l$ . The last two terms are the interactions between the atom and two driving fields, where the transition  $|f\rangle \leftrightarrow |e\rangle$  is driven by a  $\pi$ -polarized classical laser (driving amplitude  $E_{ef}$ , frequency  $\omega_{ef}$ , and phase  $\phi_{ef}$ ) and the transition  $|g\rangle \leftrightarrow |f\rangle$  is driven by a microwave field (driving amplitude  $E_{fg}$ , frequency  $\omega_{fg}$ , and phase  $\phi_{fg}$ ). In the actual experiments, the microwave driving field can be indirectly achieved by the extra Raman resonance process [72]. Therefore, the total Hamiltonian is  $H = H_s + H_d$  and all the interactions are illustrated in Fig. 1(b). For simplicity, we perform a rotating transformation defined by

$$V_1 = \exp(-i\omega_l t a^\dagger a - i\omega_e t |e\rangle\langle e| - i\omega_{fg} t |f\rangle\langle f|). \quad (3)$$

After that, the transformed Hamiltonian  $H_1 = V_1^\dagger H V_1 - iV_1^\dagger \dot{V}_1$  is rewritten as

$$H_1 = \Delta_c a^\dagger a + \omega_m b^\dagger b + \Delta_{fg} |f\rangle\langle f| + g_0 a^\dagger |g\rangle\langle e| e^{-i\Delta_l t} - ga^\dagger a(b^\dagger + b) + E_{ef} e^{i\phi_{ef}} |e\rangle\langle f| e^{i(\Delta_{ef} + \Delta_{fg})t} + E_l e^{i\phi_l} a^\dagger + E_{fg} e^{i\phi_{fg}} |f\rangle\langle g| + \text{H.c.}, \quad (4)$$

where  $\Delta_c = \omega_c - \omega_l$ ,  $\Delta_{fg} = \omega_f - \omega_{fg}$ ,  $\Delta_{ef} = \omega_e - \omega_f - \omega_{ef}$ , and  $\Delta_l = \omega_e - \omega_l$  are the corresponding detunings of different fields.

In the case of large detuning, i.e.,  $\Delta_l \gg g_0$  and  $\Delta_{ef} + \Delta_{fg} \gg E_{ef}$ , the excited state  $|e\rangle$  can be adiabatically eliminated. Then we obtain the reduced Hamiltonian

$$H_2 = \Delta_c a^\dagger a + \omega_m b^\dagger b + \Delta_f |f\rangle\langle f| - \frac{g_0^2}{\Delta_l} a^\dagger a |g\rangle\langle g| - \frac{g_0 E_{ef}}{\Delta_l} e^{i\phi_{ef}} a^\dagger |g\rangle\langle f| - ga^\dagger a(b^\dagger + b) + E_l e^{i\phi_l} a^\dagger + E_{fg} e^{i\phi_{fg}} |f\rangle\langle g| + \text{H.c.}, \quad (5)$$

where  $\Delta_f = \Delta_{fg} - E_{ef}^2/\Delta_l$  and  $E_{ef}^2/\Delta_l |f\rangle\langle f|$  is the Stark shift caused by the classical laser field  $E_{ef}$ . In addition,  $(g_0^2/\Delta_l) a^\dagger a |g\rangle\langle g|$  represents the Stark shift originating from atom-cavity coupling and  $g_0 E_{ef}/\Delta_l$  is the Raman coupling strength between the cavity and the transition  $|g\rangle \leftrightarrow |f\rangle$ . Here, for convenience, we have assumed  $\Delta_{ef} + \Delta_{fg} = \Delta_l$ , which represents the three-photon resonance. In the mechanical displacement representation defined by

$$V_2 = \exp\left(\frac{g}{\omega_m} a^\dagger a (b^\dagger - b)\right), \quad (6)$$

the nonlinear optomechanical coupling is transformed to the Kerr-like nonlinearity of the optical cavity [73]. Moreover, those phases can be renormalized after a canonical transformation  $V_3 = \exp(i\phi_l a^\dagger a - i\phi_{fg} |g\rangle\langle g|)$ . Specifically, the transformed Hamiltonian  $H_3 = V_3^\dagger V_2^\dagger H_2 V_2 V_3$  reads

$$H_3 = \Delta_c a^\dagger a + \omega_m b^\dagger b + \Delta_f |f\rangle\langle f| - \frac{g^2}{\omega_m} (a^\dagger a)^2 - \frac{g_0^2}{\Delta_l} a^\dagger a |g\rangle\langle g| - \frac{g_0 E_{ef}}{\Delta_l} e^{-i\theta} a^\dagger e^{-\frac{g}{\omega_m} (b^\dagger - b)} |g\rangle\langle f| + E_l a^\dagger e^{-(g/\omega_m)(b^\dagger - b)} + E_{fg} |f\rangle\langle g| + \text{H.c.}, \quad (7)$$

where  $g^2/\omega_m$  is the strength of the obtained Kerr-like nonlinearity and  $\theta = \phi_l - \phi_{ef} - \phi_{fg}$  is the renormalized relative phase among those external driving fields. In the actual OMSs, the single-photon optomechanical coupling is usually tiny, namely,  $g \ll \omega_m$ . Under the weak single-photon optomechanical coupling condition, the exponential factor  $\exp[-\frac{g}{\omega_m}(b^\dagger - b)]$  in Eq. (7) can be omitted safely. For this case, the Hamiltonian is decoupled into two parts, i.e., the optical part

$$H_4 = \Delta_c a^\dagger a + \Delta_f |f\rangle\langle f| - G_0 a^\dagger a |g\rangle\langle g| - G(a^\dagger a)^2 - J e^{-i\theta} a^\dagger |g\rangle\langle f| + E_l a^\dagger + E_{fg} |f\rangle\langle g| + \text{H.c.} \quad (8)$$

and the mechanical free part  $H_m = \omega_m b^\dagger b$ . For simplicity, the system parameters have been renormalized as

$$G_0 = \frac{g_0^2}{\Delta_l}, \quad G = \frac{g^2}{\omega_m}, \quad J = \frac{g_0 E_{ef}}{\Delta_l}. \quad (9)$$

Meanwhile, the dynamical evolutions of optical and mechanical parts are independent, namely,  $\exp[-i(H_4 + H_m)t]|\Psi\rangle = \exp(-iH_4 t)|\psi\rangle \otimes \exp(-iH_m t)|\psi\rangle_m$ , where  $|\Psi\rangle$ ,  $|\psi\rangle$ , and  $|\psi\rangle_m$  are the states of the whole system, the optical part, and the mechanical part, respectively. This means Eq. (8) is sufficient to study the photon statistics when we only care about the optical properties of the system.

Here the reduced Hamiltonian can be diagonalized in the relevant Hilbert space  $\{|n, g\rangle, |n-1, f\rangle\}$ . The corresponding eigenenergy then is given by

$$E_{n\pm} = \frac{(2n-1)\Delta_c + \Delta_f}{2} - \left(n^2 - n + \frac{1}{2}\right)G - \frac{n}{2}G_0 \pm \sqrt{nJ^2 + \left[\frac{(2n-1)G + nG_0}{2} - \frac{\Delta_c - \Delta_f}{2}\right]^2}. \quad (10)$$

It is easy to find that the anharmonicity of eigenenergy mainly originates from two aspects, i.e., the nonlinear optomechanical coupling and the energy splitting caused by the atom-cavity interaction. Meanwhile, we can see that the existence of the  $\Lambda$ -type atom not only shifts the energy level structure, but also changes the size of energy splitting between the higher and lower branches of eigenstates. For instance, the frequency shift and energy splitting of  $n$ -excitation eigenstates caused by the  $\Lambda$ -type atom are  $-nG_0/2$  and  $\sqrt{4nJ^2 + [(2n-1)G + nG_0 - \Delta_c + \Delta_f]^2}$ , respectively, in which the energy splitting is anharmonic and increases with the enhancements of the Stark shift strength  $G_0$  and the photon excitation number  $n$ . Hence, the photon statistics property in our proposal would be affected inevitably by the  $\Lambda$ -type atom. In the following section, the enhanced photon blockade effect is verified and discussed in detail.

### III. PHOTON STATISTICS

From the above calculation, we reduce the initial hybrid OMS with a trapped  $\Lambda$ -type atom to an atom-cavity system by utilizing the large detuning and weak optomechanical coupling conditions. Here we investigate the photon statistics property in the optical cavity via calculating its correlation function analytically and numerically. The validity of the reduced Hamiltonian in Sec. II is also proved by comparing the analytical and numerical results, where the numerical simula-

tion is carried out with the initial Hamiltonian of the hybrid OMS.

#### A. Analytical solution

The analytical solution of correlation function can be calculated via the non-Hermitian Schrödinger equation, which involves the influence of the external environment by adding phenomenologically the system decay into the reduced Hamiltonian (8). The modified non-Hermitian Hamiltonian is thus

$$H_{\text{NM}} = H_4 - i\frac{\kappa}{2}a^\dagger a, \quad (11)$$

where  $\kappa$  is the photon decay rate of the cavity. It is worth noting that we have ignored the spontaneous emission of the ground state  $|f\rangle$  due to the extremely weak strength (electric dipole forbidden). Meanwhile, the proposal still works even if the spontaneous emission of the ground state  $|f\rangle$  is considered. Substituting the Hamiltonian (11) into the Schrödinger equation  $i\partial|\psi(t)\rangle/\partial t = H_{\text{NM}}|\psi(t)\rangle$ , a set of linear differential equations about the probability amplitudes is obtained. Here  $|\psi(t)\rangle$  is the time-dependent optical state which can be expanded as

$$|\psi(t)\rangle = \sum_{n,m} C_{ng}(t)|n, g\rangle + C_{mf}(t)|m, f\rangle, \quad (12)$$

where  $C_{ng}$  and  $C_{mf}$  are the corresponding probability amplitudes of states  $|n, g\rangle$  and  $|m, f\rangle$ , respectively. Further,  $\{n, m\} \in Z$  represents the photon number in the optical cavity. Under the condition of weak driving  $\{E_l, E_{fg}\} \ll \kappa$ , the dynamical evolution of the system is confined in a low-excitation subspace, which can be truncated by a low enough photon number to solve analytically. Meanwhile, the set of differential equations for probability amplitudes is given by

$$\begin{aligned} i\frac{\partial C_{0g}}{\partial t} &= E_l C_{1g} + E_{fg} C_{0f}, \\ i\frac{\partial C_{1g}}{\partial t} &= E_l C_{0g} + \Delta_1 C_{1g} - J e^{-i\theta} C_{0f} + E_{fg} C_{1f} + \sqrt{2} E_l C_{2g}, \\ i\frac{\partial C_{0f}}{\partial t} &= E_{fg} C_{0g} - J e^{i\theta} C_{1g} + \Delta_f C_{0f} + E_l C_{1f}, \\ i\frac{\partial C_{1f}}{\partial t} &= E_{fg} C_{1g} + E_l C_{0f} + \Delta' C_{1f} - \sqrt{2} J e^{i\theta} C_{2g}, \\ i\frac{\partial C_{2g}}{\partial t} &= \sqrt{2} E_l C_{1g} - \sqrt{2} J e^{-i\theta} C_{1f} + 2\Delta_2 C_{2g}, \end{aligned} \quad (13)$$

where  $\Delta_1 = \Delta_c - i\frac{\kappa}{2} - G_0 - G$ ,  $\Delta' = \Delta_c - i\frac{\kappa}{2} + \Delta_f - G$ , and  $\Delta_2 = \Delta_c - i\frac{\kappa}{2} - G_0 - 2G$ . When the system reaches its steady state, the time-independent probability amplitudes are

approximatively solved as

$$\begin{aligned} C_{1g} &\simeq \frac{E_l J e^{-i\theta} + E_l \Delta_f}{J^2 - \Delta_f \Delta_1}, \\ C_{0f} &\simeq \frac{E_l J e^{i\theta} + E_l \Delta_1}{J^2 - \Delta_f \Delta_1}, \\ C_{1f} &\simeq \frac{E_l J e^{i\theta} C_{1g} + E_l (C_{1g} + C_{0f}) \Delta_2}{J^2 - \Delta_2 \Delta'}, \\ C_{2g} &\simeq \frac{E_l J e^{-i\theta} (C_{1g} + C_{0f}) + E_l C_{1g} \Delta'}{\sqrt{2}(J^2 - \Delta_2 \Delta')}, \end{aligned} \quad (14)$$

where we have assumed  $E_{fg} = E_l$  and  $C_{0g} \simeq 1$  and ignored the high-order small quantity due to the weak-driving condition. Generally, the photon statistics property is measured via the various correlation functions, where the single-photon blockade can be expediently characterized by the delayed second-order correlation function

$$g_2^{(2)}(\tau) = \lim_{t \rightarrow \infty} \frac{\langle a^\dagger(t) a^\dagger(t+\tau) a(t+\tau) a(t) \rangle}{\langle a^\dagger(t) a(t) \rangle \langle a^\dagger(t+\tau) a(t+\tau) \rangle}. \quad (15)$$

Here the second-order correlation function represents the probability of detecting the first photon at time  $t$  and the second photon after a time delay  $\tau$ . When the system reaches its steady state  $\rho_s = |\psi\rangle_{ss}\langle\psi|$ , the delayed second-order correlation function can be conveniently calculated by the equivalent definition

$$g_2^{(2)}(\tau) = \frac{\text{Tr}[a^\dagger a U(\tau) a \rho_s a^\dagger U^\dagger(\tau)]}{\text{Tr}(a^\dagger a \rho_s)^2}, \quad (16)$$

where  $U(\tau)$  represents the dynamical evolution operator of the system. In the following, we give the analytical expression for the steady-state zero-delay second-order correlation function

$$g_2^{(2)}(0) = \frac{\langle a^\dagger a^\dagger a a \rangle}{\langle a^\dagger a \rangle^2} \simeq \frac{2|C_{2g}|^2}{|C_{1g}|^4}, \quad (17)$$

where we have used the fact  $\{|C_{2g}|, |C_{1f}|\} \ll \{|C_{1g}|, |C_{0f}|\} \ll |C_{0g}|$  for the case of weak driving. According to the above result and the last of Eqs. (14), we can obtain the optimal parameter condition to generate the perfect photon blockade in the optical cavity. The direct expression of parameters is too cumbersome to show here, so we just give the optimal relation of those parameters as

$$J e^{-i\theta} = -\frac{(\Delta_f + J e^{-i\theta}) \Delta'}{\Delta' - G_0 + 2J \cos \theta}. \quad (18)$$

So far, we have given the analytical expression of the zero-delay second-order correlation function and recalculated the delayed second-order correlation function to characterize the photon statistics property. Moreover, the optimal parameter relation to generate the perfect photon blockade was also derived in Eq. (18), which is helpful to select the appropriate system parameters. Next we verify the above analyses via numerically simulating the system's master equation of the initial Hamiltonian.

## B. Numerical simulation

It is worth noting that the previous analytical calculation was obtained through some approximate conditions, e.g., large detuning, weak single-photon optomechanical coupling, and weak driving. So it is necessary to verify the accuracy of the above analytical results via the exact numerical simulation with the initial Hamiltonian

$$\begin{aligned} H' &= \Delta_c a^\dagger a + \omega_m b^\dagger b + \Delta_f g |f\rangle\langle f| + \Delta_l |e\rangle\langle e| \\ &\quad + g_0 e^{-i\theta} a^\dagger |g\rangle\langle e| - g a^\dagger a b^\dagger + E_l a^\dagger + E_{ef} |e\rangle\langle f| \\ &\quad + E_{fg} |f\rangle\langle g| + \text{H.c.}, \end{aligned} \quad (19)$$

where, for convenience, we have taken a transformation defined by

$$\begin{aligned} V' &= \exp(-i\omega_l t a^\dagger a - i\omega_l t |e\rangle\langle e| - i\omega_{fg} t |f\rangle\langle f|), \\ a e^{-i\phi_l} &\rightarrow a, \quad |f\rangle\langle e| e^{-i\phi_{ef}} \rightarrow |f\rangle\langle e|, \\ |g\rangle\langle f| e^{-i\phi_{fg}} &\rightarrow |g\rangle\langle f|. \end{aligned} \quad (20)$$

Here the exact numerical simulation is carried out by the method of the quantum master equation, which is written as

$$\begin{aligned} \frac{\partial \rho}{\partial t} &= -i[H', \rho] - \frac{\kappa}{2} (a^\dagger a \rho - 2a \rho a^\dagger + \rho a^\dagger a) \\ &\quad - \gamma (|e\rangle\langle e| \rho - |g\rangle\langle e| \rho |e\rangle\langle g| - |f\rangle\langle e| \rho |e\rangle\langle f| + \rho |e\rangle\langle e|) \\ &\quad - \frac{(n_{\text{th}} + 1) \gamma_m}{2} (b^\dagger b \rho - 2b \rho b^\dagger + \rho b^\dagger b) \\ &\quad - \frac{n_{\text{th}} \gamma_m}{2} (b b^\dagger \rho - 2b^\dagger \rho b + \rho b b^\dagger), \end{aligned} \quad (21)$$

where  $\gamma$  is the spontaneous emission rate of the atom, which we have assumed to be the same for the spontaneous emissions of  $|e\rangle \rightarrow |g\rangle$  and  $|e\rangle \rightarrow |f\rangle$ . In addition,  $\gamma_m$  represents the damping rate of the mechanical oscillator and  $n_{\text{th}} = [\exp(\hbar\omega_m/k_B T) - 1]^{-1}$  is the mean thermal phonon number at temperature  $T$ , where  $k_B$  is the Boltzmann constant. When the system reaches its steady-state density matrix  $\rho_s$ , the zero-delay second-order correlation function can be calculated by

$$g_2^{(2)}(0) = \frac{\text{Tr}(a^\dagger a^\dagger a a \rho_s)}{\text{Tr}(a^\dagger a \rho_s)^2}. \quad (22)$$

## C. Maximizing the single-photon occupancy

Generally, although the strong photon blockade can be obtained based on the above analysis, it is necessary to further make it occur at the single-excitation resonance to maximize the efficiency of single-photon emission. Therefore, we analyze the eigenenergy of the system to obtain its energy of single-excitation resonance, which can be directly given as

$$\begin{aligned} \varepsilon_{1\pm} &= \frac{\Delta_c + \Delta_f}{2} - \frac{G + G_0}{2} \\ &\quad \pm \sqrt{J^2 + \left(\frac{G + G_0}{2} - \frac{\Delta_c - \Delta_f}{2}\right)^2}. \end{aligned} \quad (23)$$

Applying the condition of single-excitation resonance, the optimal cavity-pumping detuning is given by

$$\Delta_c = G + G_0 + \frac{J^2}{\Delta_f} \quad (\Delta_f \neq 0), \quad (24)$$

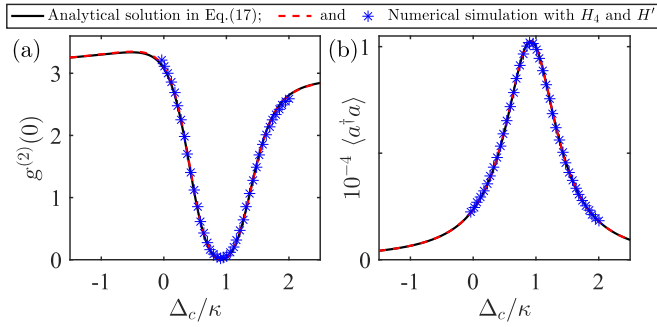


FIG. 2. (a) Zero-delay second-order correlation function  $g^{(2)}(0)$  versus the cavity-pumping field detuning  $\Delta_c$  coming from the analytical solution and the numerical simulations with different Hamiltonians. The solid black line is the analytical solution of the correlation function defined by Eq. (17), the dashed red line represents the numerical simulation from the master equation (21) with the reduced Hamiltonian in Eq. (8), and the blue asterisks show another numerical simulation with the initial Hamiltonian in Eq. (19). (b) Intracavity photon number  $\langle a^\dagger a \rangle$  versus the cavity-pumping field detuning  $\Delta_c$ .

which will maximize the single-photon occupancy (equivalent to the high efficiency of single-photon emission). Combining the optimal cavity-pumping detuning and the previous optimal parameter relation in Eq. (18), we can obtain the strong photon blockade and the high single-photon occupancy at the same time, which means a high-quality and efficient single-photon source is generated. Different from Ref. [58], the anharmonic eigenenergy spectrum modified by the trapped  $\Lambda$ -type atom provides the possibility to manipulate the position of the optimal photon blockade without changing the optomechanical coupling strength.

Next we solve the second-order correlation function with the optimal condition via the analytical result in Eq. (17) and via the numerical simulation from Eq. (21) to validate our calculations, as shown in Fig. 2(a). For comparison, we also give the numerical simulation with the reduced Hamiltonian in Eq. (8). In the above calculations, the system parameters were selected appropriately based on the experiments in [74–76],

e.g.,  $\kappa = 2\pi$  MHz,  $g_0/\kappa = 10$ , and  $\gamma/\kappa = 0.5$ , where the atom-cavity coupling belongs to the strong-coupling region. In addition, the parameters of the mechanical oscillator are set as  $\omega_m/\kappa = 100$ ,  $g/\omega_m = 0.03$ , and  $\gamma_m/\omega_m = 10^{-6}$ , which is a high- $Q$  resonator. The external drivings are chosen appropriately as  $\Delta_l/\kappa = 100$ ,  $E_l/\kappa = E_{fg}/\kappa = 0.01 \ll 1$ , and  $\Delta_f/\kappa = -0.5$ . The temperature of the system is precooled to  $T = 1$  mK. The  $E_{ef}$  and the relative phase  $\theta$  are chosen according to the optimal relation in Eq. (18). We can see that the analytical solution agrees well with those numerical simulations in the vicinity of the occurring photon blockade. Further, the correlation function is nearly zero at the optimal detuning given in Eq. (24), which indicates the appearance of a strong photon blockade. We also show the intracavity photon number  $\langle a^\dagger a \rangle \simeq |C_{1g}|^2$  versus the cavity-pumping detuning with the optimal system parameters, as shown in Fig. 2(b). We can see that the intracavity photon number reaches its peak value (related to the driving amplitudes and about  $E_l^2/\kappa^2$ ) at the optimal detuning, which implies that the single-photon occupancy is highest at this time. Here the analytical result of the intracavity photon number is also identical to those numerical simulations. Therefore, a strong photon blockade is achieved and a high occupancy probability of single-photon excitation is also obtained at the same time.

#### D. Discussion

Here we discuss the effect of parameter fluctuation on photon blockade according to the foregoing analysis. We take the detuning  $\Delta_f$  as an example to explore its effect on photon blockade. Figure 3(a) shows the variation of the zero-delay second-order correlation function  $g^{(2)}(0)$  with the detuning  $\Delta_f$  and  $\Delta_c$  via numerically simulation. We find that the location of the perfect photon blockade occurring changes with the detuning  $\Delta_f$  when the optimal condition is satisfied. However, we also notice that the photon blockade vanishes in the vicinity of  $\Delta_f/\kappa = 0$ , which means that the detuning of the microwave field cannot be equal to the Stark shift of level  $|f\rangle$  and is consistent with the analytical calculation in Eq. (24). Furthermore, the dashed white line represents the analytical location of a perfect photon blockade appearing, which is

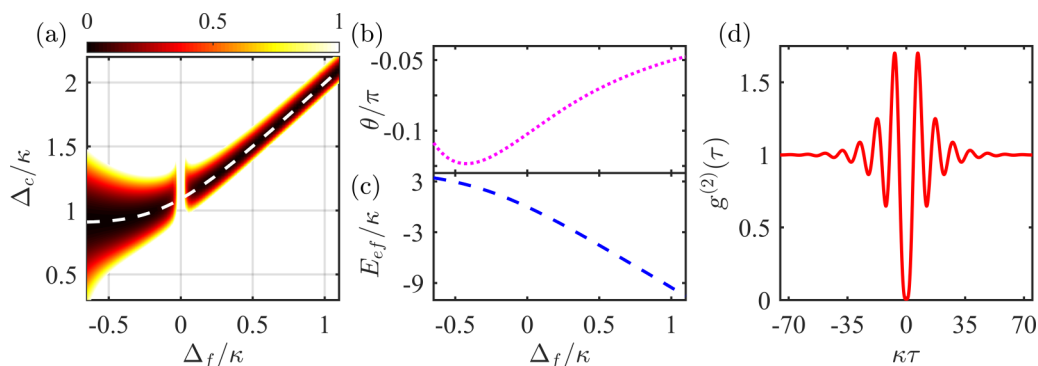


FIG. 3. (a) Zero-delay second-order correlation function  $g^{(2)}(0)$  versus the detuning  $\Delta_f$  and  $\Delta_c$  via numerically simulating the master equation. The dashed white line represents the location of the perfect photon blockade, which comes from the analytical result in Eq. (24). Also shown are the (b) optimal relative phase  $\theta$  and (c) driving amplitude  $E_{ef}$  versus the detuning  $\Delta_f$ , which are obtained by solving Eq. (18). (d) Delayed second-order correlation function  $g^{(2)}(\tau)$  versus the delay time, which is calculated by the definition in Eq. (16).

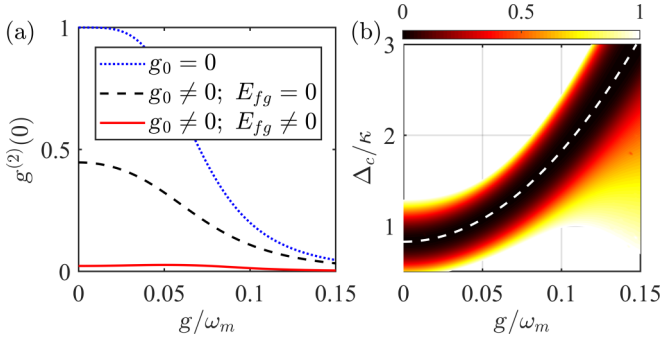


FIG. 4. (a) Zero-delay second-order correlation function  $g^{(2)}(0)$  versus the single-photon optomechanical coupling  $g$  for the atom and microwave field existing or not. (b) Correlation function  $g^{(2)}(0)$  changing with the optomechanical coupling  $g$  and cavity-pumping detuning  $\Delta_c$ , which can also describe the change of the perfect photon blockade location caused by the optomechanical coupling. The dashed white line is the relation between the blockade location and optomechanical coupling obtained by Eq. (24).

identical to the trend of numerical simulation. The optimal relative phase  $\theta$  and driving amplitude  $E_{ef}$  are calculated and shown in Figs. 3(b) and 3(c), respectively. Significantly, the classical driving  $E_{ef}$  does not need to satisfy the above weak-driving assumption ( $|E_{ef}/\kappa| > 1$ ) in our scheme. This is because the transition  $|f\rangle \leftrightarrow |e\rangle$  is suppressed due to the large-detuning condition  $\Delta_{ef} \gg E_{ef}$ . Moreover, we also calculate the delayed second-order correlation function  $g^{(2)}(\tau)$  according to the definition given in Eq. (16) and the result is shown in Fig. 3(d). As we can see, the delayed second-order correlation function is always larger than the zero-delay one, which indicates that the photon is an antibunching state and tends to be emitted one by one. When the delay time is long enough, the delayed correlation function reaches 1 and the photon is a standard Poisson distribution.

Crucially, we discuss the effect of optomechanical coupling on photon blockade. In the usual OMSs, the strong photon blockade requires a very large single-photon optomechanical coupling [see the dotted blue line in Fig. 4(a)], which has been difficult to achieve in recent experiments. Different from the schemes assisted by harmonic cavity [56,57], we study the effect of the  $\Lambda$ -type atom on photon blockade and find that the  $\Lambda$ -type atom not only shifts the energy level structure, but also changes the size of the energy splitting between the higher and lower branches of eigenstates. Therefore, a new anharmonicity is introduced into the eigenenergy of the system. Through numerically simulating Eq. (21), we obtain an enhanced photon blockade effect when the microwave field is nonexistent [see the dashed black line in Fig. 4(a)]. However, the enhanced photon blockade effect is not satisfactory when the single-photon optomechanical coupling is small, which means that the excessively large optomechanical coupling is still necessary to achieve the strong photon blockade effect. Fortunately, the photon blockade effect can be further enhanced significantly via the microwave driving field [see the solid red line in Fig. 4(a)], where a satisfactory photon blockade is obtained. We note further that the correlation function is not strictly equal to 0 when the single-photon optomechanical coupling is too small ( $g/\omega_m < 0.1$ ). This is because of the

inherent disadvantage of suppressing multiphoton excitation incompletely in the unconventional photon blockade mechanism. However, the photon blockade phenomenon gradually becomes perfect [ $g^{(2)}(0) \simeq 0$ ] with the optomechanical coupling increasing. In the above simulations, we have selected the single-excitation resonant condition  $\Delta_c = G$  or  $\Delta_c = G + G_0 + J^2/\Delta_f$ , which respectively corresponds to the atom existing or not. Furthermore, we also discuss the influence of optomechanical coupling on the optimal blockade location, as shown in Fig. 4(b). We find that the optimal blockade location is related to optomechanical coupling, which can also be demonstrated by Eqs. (9) and (24). However, it is worth noting that the optomechanical coupling has no impact on the selection of those optimal parameters [substituting Eq. (24) into Eq. (18)]. We thus can conclude that the optomechanical coupling just changes the location of the strong photon blockade occurring.

In the preceding discussion we investigated the generation of strong photon blockade and found that the photon blockade effect is only slightly enhanced when the microwave field is nonexistent. Here we analyze the reason for this phenomenon via calculating the photon statistics without the microwave field ( $E_{fg} = 0$ ). Meanwhile, the probability amplitudes in Eq. (12) can be similarly solved and written as

$$\begin{aligned}
 C_{1g} &\simeq \frac{E_l \Delta_f}{J^2 - \Delta_f \Delta_1}, \\
 C_{0f} &\simeq \frac{E_l J e^{i\theta}}{J^2 - \Delta_f \Delta_1}, \\
 C_{1f} &\simeq \frac{E_l J e^{i\theta} C_{1g} + E_l C_{0f} \Delta_2}{J^2 - \Delta_2 \Delta'}, \\
 C_{2g} &\simeq \frac{E_l J e^{-i\theta} C_{0f} + E_l C_{1g} \Delta'}{\sqrt{2}(J^2 - \Delta_2 \Delta')}. \quad (25)
 \end{aligned}$$

It is easy to confirm that we cannot derive the real solution of the equation  $|C_{2g}| = 0$ , i.e.,  $J^2 + \Delta_f(\Delta_c - i_k^2 + \Delta_f - G) = 0$ , which means the perfect photon blockade cannot be generated in the absence of the microwave field  $E_{fg}$ . However, it is worth emphasizing that the photon blockade still exists due to  $g^{(2)}(0) < 1$ , which is possible with appropriate system parameters, as shown in Fig. 5(a). In Fig. 5(b), the dynamical evolution of the correlation function is shown to verify the above analysis under the steady-state assumption. We also discuss the dynamical evolution of the intracavity photon number when the microwave driving exists or does not, and the results are shown in Fig. 5(c). We can see that the single-photon occupancy is higher when the microwave driving is nonexistent. That means the better blockade effect corresponds to the lower intracavity photon number. In order to get a perfect photon blockade effect, we must sacrifice the intracavity photon number and the microwave driving is necessary. Finally, the delayed second-order correlation function  $g^{(2)}(\tau)$  is shown in Fig. 5(d) when the microwave driving field is existent or not. We find that the delayed second-order correlation function is always low in the presence of microwave driving field, which further shows the promoting effect of the microwave driving field on photon blockade.

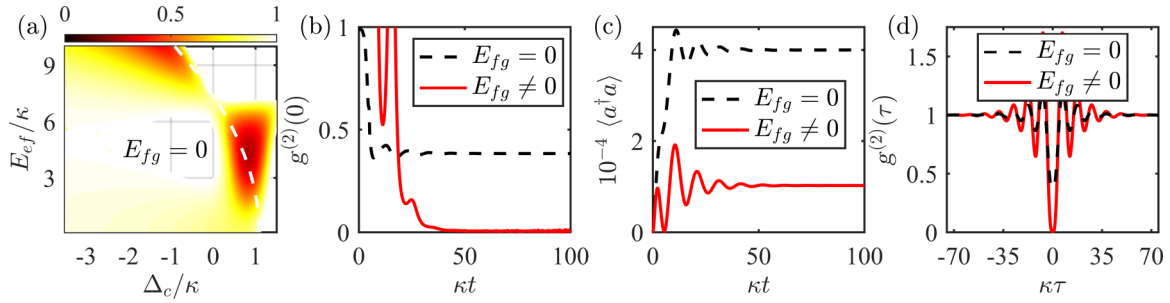


FIG. 5. (a) Zero-delay second-order correlation function  $g_g^{(2)}(0)$  versus the cavity-pumping detuning  $\Delta_c$  and the driving amplitude  $E_{ef}$  when the microwave field is nonexistent ( $E_{fg} = 0$ ). Also shown are the dynamical evolutions of (b) the zero-delay second-order correlation function  $g_g^{(2)}(0)$  and (c) the intracavity photon number  $\langle a^\dagger a \rangle$  with or without the microwave driving field  $E_{fg}$ . (d) Delayed second-order correlation function  $g_g^{(2)}(\tau)$  with or without the microwave driving field.

#### IV. CONCLUSION

We have proposed a promising scheme to investigate the photon statistics in a hybrid OMS with a trapped  $\Lambda$ -type atom, in which a microwave field is utilized to drive the atomic transition. The strong photon blockade effect can be achieved even with a weak optomechanical coupling and it is measured by the usual second-order correlation function, which is calculated via analytically solving the Schrödinger equation and numerically simulating the quantum master equation. Specifically, when the weak microwave field and nonresonant coupled  $\Lambda$ -type atom satisfy the derived optimal parameter relation, the strong photon blockade can be achieved, which breaks the strong-coupling limitation in usual OMSs. This is because the interplay of the nonresonant coupled atom and microwave driving field is conducive to suppressing the two-photon excitation completely, thus resulting in the enhancement of the photon blockade effect. We also demonstrated analytically that the photon blockade is imperfect

when the microwave field is nonexistent. Moreover, in order to improve the efficiency of single-photon emission in our scheme, we selected the single-excitation resonant condition to maximize the occupancy probability of single-photon excitation when the strong photon blockade occurs. Therefore, a high-quality and efficient single-photon source can be generated. Our work explores the feasibility of a strong photon blockade occurring with a weak single-photon optomechanical coupling and might have application in generating the few-photon quantum states.

#### ACKNOWLEDGMENTS

We would like to thank L. Qi, S. Khan, R. Huang, and W. Zhang for helpful discussions. This work was supported by the National Natural Science Foundation of China under Grants No. 61822114, No. 61575055, No. 11874132, No. 12074330, and No. 62071412.

- [1] M. Aspelmeyer, T. J. Kippenberg, and F. Marquardt, *Rev. Mod. Phys.* **86**, 1391 (2014).
- [2] L. F. Wei, Y. X. Liu, C. P. Sun, and F. Nori, *Phys. Rev. Lett.* **97**, 237201 (2006).
- [3] T. J. Kippenberg and K. J. Vahala, *Opt. Express* **15**, 17172 (2007).
- [4] C. Dong, J. Zhang, V. Fiore, and H. Wang, *Optica* **1**, 425 (2014).
- [5] M. Poot and H. S. van der Zant, *Phys. Rep.* **511**, 273 (2012).
- [6] J. Millen, T. S. Monteiro, R. Pettit, and A. N. Vamivakas, *Rep. Prog. Phys.* **83**, 026401 (2020).
- [7] D. J. Wilson, V. Sudhir, N. Piro, R. Schilling, A. Ghadimi, and T. J. Kippenberg, *Nature (London)* **524**, 325 (2015).
- [8] I. Wilson-Rae, N. Nooshi, W. Zwerger, and T. J. Kippenberg, *Phys. Rev. Lett.* **99**, 093901 (2007).
- [9] Y. M. Liu, C. H. Bai, D. Y. Wang, T. Wang, M. H. Zheng, H. F. Wang, A. D. Zhu, and S. Zhang, *Opt. Express* **26**, 6143 (2018).
- [10] T. Rocheleau, T. Ndukum, C. Macklin, J. B. Hertzberg, A. A. Clerk, and K. C. Schwab, *Nature (London)* **463**, 72 (2009).
- [11] D. G. Lai, F. Zou, B. P. Hou, Y. F. Xiao, and J. Q. Liao, *Phys. Rev. A* **98**, 023860 (2018).
- [12] D. Y. Wang, C. H. Bai, S. Liu, S. Zhang, and H. F. Wang, *Phys. Rev. A* **98**, 023816 (2018).
- [13] E. E. Wollman, C. U. Lei, A. J. Weinstein, J. Suh, A. Kronwald, F. Marquardt, A. A. Clerk, and K. C. Schwab, *Science* **349**, 952 (2015).
- [14] T. P. Purdy, P.-L. Yu, R. W. Peterson, N. S. Kampel, and C. A. Regal, *Phys. Rev. X* **3**, 031012 (2013).
- [15] W. J. Gu and G. X. Li, *Opt. Express* **21**, 20423 (2013).
- [16] C. H. Bai, D. Y. Wang, S. Zhang, S. Liu, and H. F. Wang, *Photon. Res.* **7**, 1229 (2019).
- [17] D. Vitali, S. Gigan, A. Ferreira, H. R. Böhm, P. Tombesi, A. Guerreiro, V. Vedral, A. Zeilinger, and M. Aspelmeyer, *Phys. Rev. Lett.* **98**, 030405 (2007).
- [18] C. F. Ockeloen-Korppi, E. Damskägg, J.-M. Pirkkalainen, M. Asjad, A. A. Clerk, F. Massel, M. J. Woolley, and M. A. Sillanpää, *Nature (London)* **556**, 478 (2018).
- [19] J.-Q. Liao and L. Tian, *Phys. Rev. Lett.* **116**, 163602 (2016).
- [20] B. Xiong, X. Li, S.-L. Chao, Z. Yang, W.-Z. Zhang, and L. Zhou, *Opt. Express* **27**, 13547 (2019).
- [21] H. Tan, F. Bariani, G. Li, and P. Meystre, *Phys. Rev. A* **88**, 023817 (2013).
- [22] Y. Li, Y. Y. Huang, X. Z. Zhang, and L. Tian, *Opt. Express* **25**, 18907 (2017).

- [23] C. Jiang, B. Ji, Y. Cui, F. Zuo, J. Shi, and G. Chen, *Opt. Express* **26**, 15255 (2018).
- [24] G. S. Agarwal and S. Huang, *Phys. Rev. A* **81**, 041803(R) (2010).
- [25] S. Weis, R. Rivière, S. Deléglise, E. Gavartin, O. Arcizet, A. Schliesser, and T. J. Kippenberg, *Science* **330**, 1520 (2010).
- [26] S. Shahidani, M. H. Naderi, and M. Soltanolkotabi, *Phys. Rev. A* **88**, 053813 (2013).
- [27] X. B. Yan, *Phys. Rev. A* **101**, 043820 (2020).
- [28] I. M. Mirza, W. Ge, and H. Jing, *Opt. Express* **27**, 25515 (2019).
- [29] A. Settineri, V. Macrì, L. Garziano, O. Di Stefano, F. Nori, and S. Savasta, *Phys. Rev. A* **100**, 022501 (2019).
- [30] P. Rabl, *Phys. Rev. Lett.* **107**, 063601 (2011).
- [31] A. Nunnenkamp, K. Børkje, and S. M. Girvin, *Phys. Rev. Lett.* **107**, 063602 (2011).
- [32] J. Q. Liao and F. Nori, *Phys. Rev. A* **88**, 023853 (2013).
- [33] C. Zhai, R. Huang, H. Jing, and L. M. Kuang, *Opt. Express* **27**, 27649 (2019).
- [34] D.-Y. Wang, C.-H. Bai, S. Liu, S. Zhang, and H.-F. Wang, *New J. Phys.* **22**, 093006 (2020).
- [35] R. Huang, A. Miranowicz, J.-Q. Liao, F. Nori, and H. Jing, *Phys. Rev. Lett.* **121**, 153601 (2018).
- [36] B. Li, R. Huang, X. Xu, A. Miranowicz, and H. Jing, *Photon. Res.* **7**, 630 (2019).
- [37] P. Yang, M. Li, X. Han, H. He, G. Li, C.-L. Zou, P. Zhang, and T. Zhang, [arXiv:1911.10300](https://arxiv.org/abs/1911.10300).
- [38] W. M. Witzel, A. Shabaev, C. S. Hellberg, V. L. Jacobs, and A. L. Efros, *Phys. Rev. Lett.* **105**, 137401 (2010).
- [39] K. R. Motes, J. P. Olson, E. J. Rabeaux, J. P. Dowling, S. J. Olson, and P. P. Rohde, *Phys. Rev. Lett.* **114**, 170802 (2015).
- [40] L. Tian and H. J. Carmichael, *Phys. Rev. A* **46**, R6801 (1992).
- [41] W. Leoński and R. Tanaś, *Phys. Rev. A* **49**, R20 (1994).
- [42] A. Imamoglu, H. Schmidt, G. Woods, and M. Deutsch, *Phys. Rev. Lett.* **79**, 1467 (1997).
- [43] K. M. Birnbaum, A. Boca, R. Miller, A. D. Boozer, T. E. Northup, and H. J. Kimble, *Nature (London)* **436**, 87 (2005).
- [44] A. J. Hoffman, S. J. Srinivasan, S. Schmidt, L. Spietz, J. Aumentado, H. E. Türeci, and A. A. Houck, *Phys. Rev. Lett.* **107**, 053602 (2011).
- [45] T. C. H. Liew and V. Savona, *Phys. Rev. Lett.* **104**, 183601 (2010).
- [46] H. Z. Shen, Y. H. Zhou, and X. X. Yi, *Phys. Rev. A* **91**, 063808 (2015).
- [47] H. Z. Shen, Y. H. Zhou, H. D. Liu, G. C. Wang, and X. X. Yi, *Opt. Express* **23**, 32835 (2015).
- [48] F. Zou, D. G. Lai, and J. Q. Liao, *Opt. Express* **28**, 16175 (2020).
- [49] M. Bajcsy, A. Majumdar, A. Rundquist, and J. Vučković, *New J. Phys.* **15**, 025014 (2013).
- [50] J. Li, C. Ding, and Y. Wu, *Phys. Rev. A* **100**, 033814 (2019).
- [51] J. Tang, Y. Deng, and C. Lee, *Phys. Rev. Appl.* **12**, 044065 (2019).
- [52] H. J. Sijnders, J. A. Frey, J. Norman, H. Flayac, V. Savona, A. C. Gossard, J. E. Bowers, M. P. van Exter, D. Bouwmeester, and W. Löffler, *Phys. Rev. Lett.* **121**, 043601 (2018).
- [53] C. Vaneph, A. Morvan, G. Aiello, M. Féchant, M. Aprili, J. Gabelli, and J. Estève, *Phys. Rev. Lett.* **121**, 043602 (2018).
- [54] K. Stannigel, P. Komar, S. J. M. Habraken, S. D. Bennett, M. D. Lukin, P. Zoller, and P. Rabl, *Phys. Rev. Lett.* **109**, 013603 (2012).
- [55] P. Kómár, S. D. Bennett, K. Stannigel, S. J. M. Habraken, P. Rabl, P. Zoller, and M. D. Lukin, *Phys. Rev. A* **87**, 013839 (2013).
- [56] X. W. Xu and Y. J. Li, *J. Phys. B* **46**, 035502 (2013).
- [57] B. Sarma and A. K. Sarma, *Phys. Rev. A* **98**, 013826 (2018).
- [58] D. Y. Wang, C. H. Bai, X. Han, S. Liu, S. Zhang, and H. F. Wang, *Opt. Lett.* **45**, 2604 (2020).
- [59] Y. X. Liu, A. Miranowicz, Y. B. Gao, J. Bajer, C. P. Sun, and F. Nori, *Phys. Rev. A* **82**, 032101 (2010).
- [60] N. Didier, S. Pugnetti, Y. M. Blanter, and R. Fazio, *Phys. Rev. B* **84**, 054503 (2011).
- [61] A. Miranowicz, J. Bajer, N. Lambert, Y. X. Liu, and F. Nori, *Phys. Rev. A* **93**, 013808 (2016).
- [62] X. Wang, A. Miranowicz, H. R. Li, and F. Nori, *Phys. Rev. A* **93**, 063861 (2016).
- [63] H. Wang, X. Gu, Y. X. Liu, A. Miranowicz, and F. Nori, *Phys. Rev. A* **92**, 033806 (2015).
- [64] B. Sarma and A. K. Sarma, *J. Phys. B* **51**, 075505 (2018).
- [65] T. Holz, R. Betzholz, and M. Bienert, *Phys. Rev. A* **92**, 043822 (2015).
- [66] J. Restrepo, I. Favero, and C. Ciuti, *Phys. Rev. A* **95**, 023832 (2017).
- [67] D. Y. Wang, C. H. Bai, H. F. Wang, A. D. Zhu, and S. Zhang, *Sci. Rep.* **6**, 24421 (2016).
- [68] D. A. Steck, Rubidium 87 D line data, <http://steck.us/alkalidata>
- [69] S. L. Su, Q. Guo, H. F. Wang, and S. Zhang, *Phys. Rev. A* **92**, 022328 (2015).
- [70] M. Mücke, J. Bochmann, C. Hahn, A. Neuzner, C. Nölleke, A. Reiserer, G. Rempe, and S. Ritter, *Phys. Rev. A* **87**, 063805 (2013).
- [71] J. Q. You and F. Nori, *Nature (London)* **474**, 589 (2011).
- [72] Y. J. Lin, K. Jiménez-García, and I. B. Spielman, *Nature (London)* **471**, 83 (2011).
- [73] D. Y. Wang, C. H. Bai, S. Liu, S. Zhang, and H. F. Wang, *Phys. Rev. A* **99**, 043818 (2019).
- [74] J. Volz, R. Gehr, G. Dubois, J. Estève, and J. Reichel, *Nature (London)* **475**, 210 (2011).
- [75] Y. Sato, Y. Tanaka, J. Upham, Y. Takahashi, T. Asano, and S. Noda, *Nat. Photon.* **6**, 56 (2012).
- [76] S. M. Spillane, T. J. Kippenberg, K. J. Vahala, K. W. Goh, E. Wilcut, and H. J. Kimble, *Phys. Rev. A* **71**, 013817 (2005).